Chapter 8: Anthropogenic and Natural Radiative Forcing

Coordinating Lead Authors: Gunnar Myhre (Norway), Drew Shindell (USA)

Lead Authors: François-Marie Bréon (France), William Collins (UK), Jan Fuglestvedt (Norway), Jianping Huang (China), Dorothy Koch (USA), Jean-François Lamarque (USA), David Lee (UK), Blanca Mendoza (Mexico), Teruyuki Nakajima (Japan), Alan Robock (USA), Graeme Stephens (USA), Toshihiko Takemura (Japan), Hua Zhang (China)

Contributing Authors: Olivier Boucher (France), Stig B. Dalsøren (Norway), John Daniel (USA), Piers Forster (UK), Claire Granier (France), Joanna Haigh (UK), Jed O. Kaplan (Switzerland), Brian, O'Neill (USA), Glen Peters (Norway), Julia Pongratz (Germany), Venkatachalam Ramaswamy (USA), Leon Rotstayn (Australia), Paul Young (USA), Jean-Paul Vernier (USA)

Review Editors: Daniel Jacob (USA), A.R. Ravishankara (USA), Keith Shine (UK)

Date of Draft: 5 October 2012

Notes: TSU Compiled Version

Table of Contents

8.SM: Supplementary Material

8.SM.1 Atmospheric Chemistry

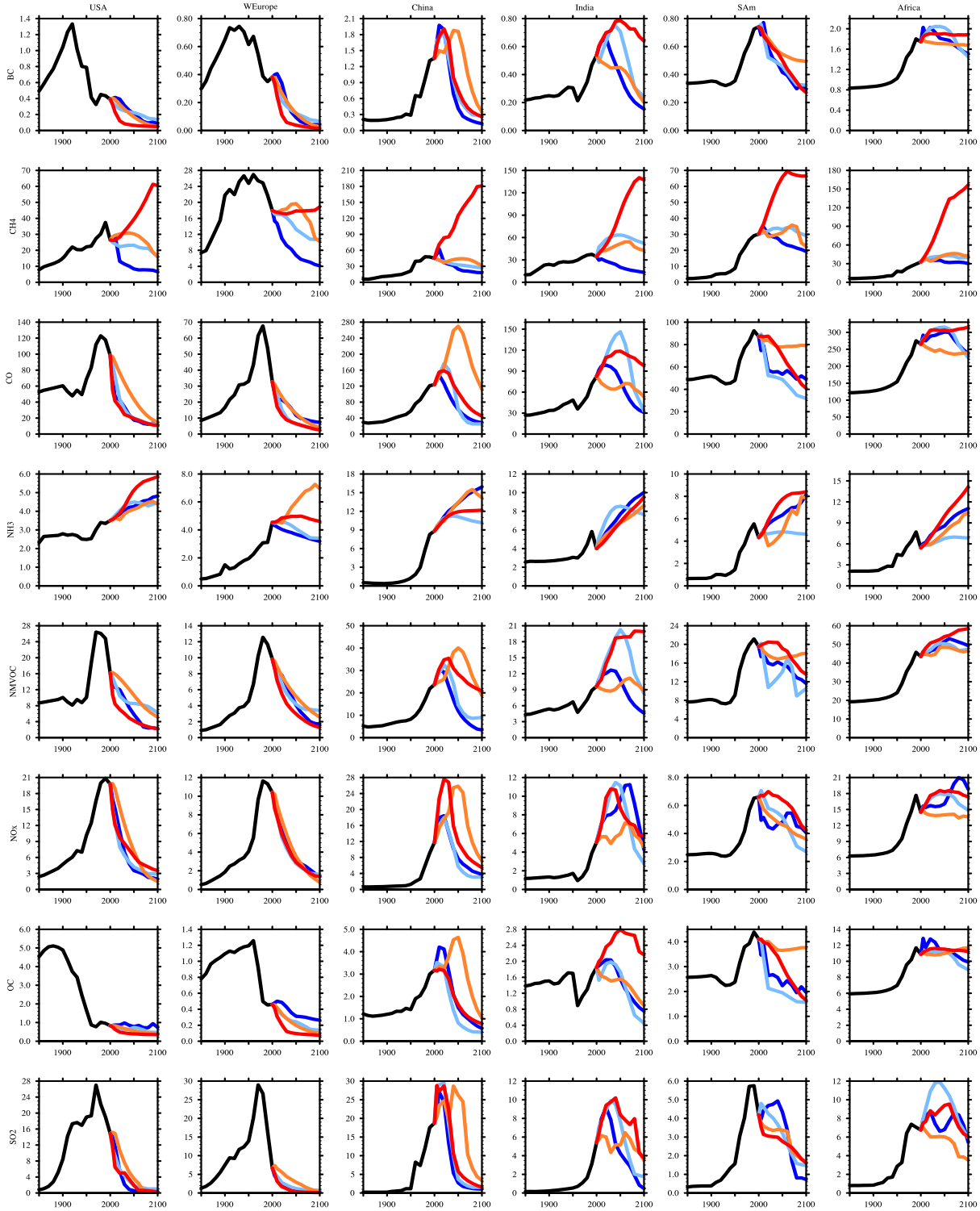

Figure 8.SM.1: Time evolution of regional (Africa, China, India, North America, South America and Western Europe) anthropogenic and biomass burning emissions 1850–2100 used in CMIP5/ACCMIP following each RCP; blue (RCP2.6), light blue (RCP4.5), orange (RCP6.0) and red (RCP8.5). BC stands for black carbon (in Tg(C) yr^{-1}), OC for organic carbon (in Tg(C) yr^{-1}), NMVOC for non-methane volatile organic compounds (in Tg(C) yr^{-1}) and NO_X for nitrogen oxides (in Tg(NO_2) yr^{-1}). Other panels are in Tg(species) yr^{-1}. Historical (1850–2000) values are from Lamarque et al. (2010). RCP values are from van Vuuren et al. (2011).

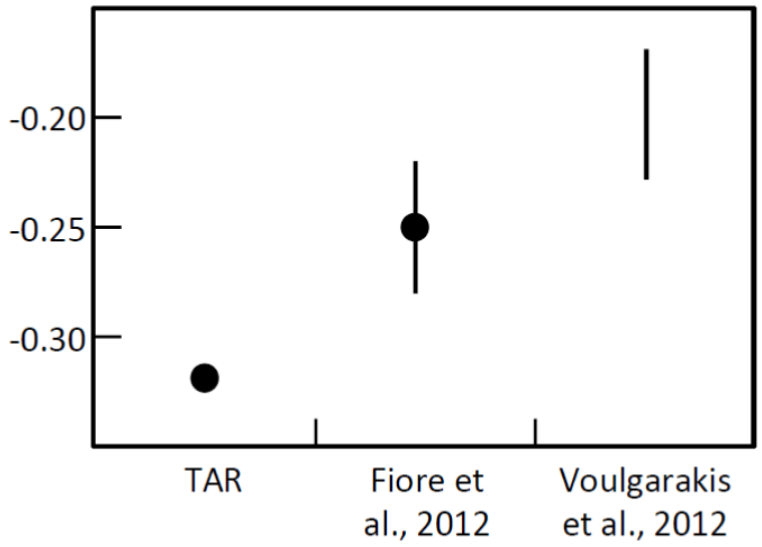

Figure 8.SM.2: Calculated OH feedback, Δln(OH)/Δ(ln(CH4)). A value of X indicates a X% change in OH for a 1% increase in CH4.

8.SM.2 Natural Radiative Forcing Changes: Solar and Volcanic

8.SM.2.1 TSI Variations Since Preindustrial Time

Table 8.SM.1: Reconstruction of Total Solar Irradiance (W m^{-2}) from Vieira et al. (2011). Series matching PMOD at 1976 and between 1976 and 2011 values are substituted by PMOD data. PMOD is already matched to TIM at 2003.

Year	TSI	Year	TSI	Year	TSI
1745	1360.41963				
1746	1360.42277				
1747	1360.39671				
1748	1360.62622				
1749	1360.90734				
1750	1360.92873				
1751	1360.82872	1851	1361.04306	1951	1361.19713
1752	1360.71622	1852	1361.0773	1952	1361.25719
1753	1360.68734	1853	1361.0052	1953	1361.10885
1754	1360.61605	1854	1360.85739	1954	1360.94758
1755	1360.53713	1855	1360.73137	1955	1361.04117
1756	1360.52947	1856	1360.65543	1956	1361.39282
1757	1360.58001	1857	1360.65743	1957	1361.86851
1758	1360.56523	1858	1360.78464	1958	1362.34774
1759	1360.18479	1859	1360.88036	1959	1362.09047
1760	1360.11428	1860	1361.14299	1960	1362.0294
1761	1360.81235	1861	1361.18878	1961	1361.73413
1762	1360.87967	1862	1361.02265	1962	1361.29834
1763	1360.7969	1863	1360.9699	1963	1361.20726
1764	1360.77015	1864	1360.80378	1964	1361.07035
1765	1360.53669	1865	1360.79503	1965	1360.98631
1766	1360.57884	1866	1360.77546	1966	1361.01372
1767	1360.66725	1867	1360.66178	1967	1361.32966
1768	1361.04794	1868	1360.64683	1968	1361.55742

1769	1361.29242	1869	1360.88956	1969	1361.49251
1770	1361.51797	1870	1360.72281	1970	1361.60293
1771	1361.33057	1871	1361.11079	1971	1361.52787
1772	1361.30971	1872	1361.01714	1972	1361.48148
1773	1361.0439	1873	1361.03777	1973	1361.24829
1774	1360.91624	1874	1360.92984	1974	1361.09827
1775	1360.64981	1875	1360.81734	1975	1360.97256
1776	1360.60225	1876	1360.71778	1976	1360.90646
1777	1360.66458	1877	1360.68863	1977	1361.01683
1778	1361.05031	1878	1360.63011	1978	1361.37899
1779	1360.6797	1879	1360.60746	1979	1361.79164
1780	1360.42494	1880	1360.64195	1980	1361.91109
1781	1360.51047	1881	1360.87894	1981	1361.88633
1782	1360.72436	1882	1360.78925	1982	1361.55552
1783	1360.45186	1883	1360.70511	1983	1361.54358
1784	1360.50096	1884	1361.0595	1984	1361.10936
1785	1360.58973	1885	1360.94618	1985	1360.96418
1786	1360.76577	1886	1360.82697	1986	1360.97111
1787	1360.92449	1887	1360.69152	1987	1361.05984
1788	1361.17469	1888	1360.65953	1988	1361.36771
1789	1360.68725	1889	1360.62719	1989	1361.849
1790	1360.50846	1890	1360.62668	1990	1361.79486
1791	1360.51987	1891	1360.78478	1991	1361.76574
1792	1360.55979	1892	1360.96103	1992	1361.54537
1793	1360.45392	1893	1361.18518	1993	1361.24573
1794	1360.46179	1894	1361.45384	1994	1361.088
1795	1360.73056	1895	1361.30592	1995	1360.97615
1796	1360.68651	1896	1361.09334	1996	1360.87825
1797	1360.61358	1897	1360.90705	1997	1361.03642
1798	1360.60313	1898	1360.83966	1998	1361.37468
1799	1360.58322	1899	1360.80601	1999	1361.59444
1800	1360.52728	1900	1360.72687	2000	1361.79853
1801	1360.77306	1901	1360.6146	2001	1361.7408
1802	1360.85932	1902	1360.58215	2002	1361.77545
1803	1360.68805	1903	1360.66409	2003	1361.308
1804	1360.63541	1904	1361.00602	2004	1361.09839
1805	1360.59295	1905	1360.81171	2005	1360.92418
1806	1360.66276	1906	1361.13113	2006	1360.83155
1807	1360.51135	1907	1360.92365	2007	1360.72422
1808	1360.45292	1908	1361.07309	2008	1360.66634
1809	1360.45678	1909	1360.91725	2009	1360.65172
1810	1360.42039	1910	1360.88464	2010	1360.85473
1811	1360.40544	1911	1360.69538	2011	1361.06602
1812	1360.40452	1912	1360.60179		
1813	1360.42309	1913	1360.62238		
1814	1360.46094	1914	1360.68608		
1815	1360.47597	1915	1361.02614		
1816	1360.54618	1916	1361.42676		
1817	1360.57668	1917	1361.55595		
1818	1360.5415	1918	1361.81444		

1819	1360.53133	1919	1361.4594
1820	1360.49646	1920	1361.21527
1821	1360.45451	1921	1361.01861
1822	1360.44724	1922	1360.83107
1823	1360.43185	1923	1360.74954
1824	1360.49649	1924	1360.71823
1825	1360.5508	1925	1360.81606
1826	1360.60875	1926	1361.07658
1827	1360.79773	1927	1361.39145
1828	1360.87169	1928	1361.16722
1829	1360.88493	1929	1361.13545
1830	1360.93948	1930	1361.27779
1831	1360.93938	1931	1360.99105
1832	1360.78572	1932	1360.81219
1833	1360.67712	1933	1360.7209
1834	1360.65075	1934	1360.73086
1835	1360.68957	1935	1360.87177
1836	1361.05533	1936	1361.42165
1837	1361.32852	1937	1361.57663
1838	1361.30317	1938	1361.51524
1839	1361.13263	1939	1361.61805
1840	1361.12796	1940	1361.43764
1841	1360.98029	1941	1361.34311
1842	1360.8863	1942	1361.1495
1843	1360.83084	1943	1360.89022
1844	1360.75526	1944	1360.85241
1845	1360.73908	1945	1361.06793
1846	1360.75644	1946	1361.10843
1847	1360.47347	1947	1361.6089
1848	1360.79665	1948	1361.99751
1849	1361.24322	1949	1361.82813
1850	1361.10688	1950	1361.72814

8.SM.2.2 TSI Variations Since Maunder Minimum

For the MM-to-present AR4 gives a RF range of 0.1–0.28 W m^{-2}, equivalent to 0.08–0.22 W m^{-2} used here. The estimates based on irradiance changes in Sun-like stars were included in this range but are not included in the AR5 range because they are now considered incorrect: Baliunas and Jastrow (1990) found a bimodal separation between non-cycling MM-type stars with the lowest Ca II brightness, and the higher emission Ca II cycling stars. More recent surveys have not reproduced their results and suggest that the selection of the original set was flawed (Wright, 2004); also, stars in a MM-like state do not always exhibit Ca II emission brightness below that of solar minimum (Hall and Lockwood, 2004).

The reconstructions in Schmidt et al. (2011) indicate a MM-to-present RF range of 0.08–0.18 W m^{-2}, which is within the AR4 range although narrower. Gray et al. (2010) point out that choosing the solar activity minima years of 1700 (Maunder) or 1800 (Dalton) would substantially increase the solar RF with respect to 1750-to-present while leaving the anthropogenic forcings essentially unchanged, and that these solar minima forcings would represent better the solar RF of the preindustrial era.

Other recent estimates give various MM-to-present RF values: The analysis of Shapiro et al (2011) falls outside the range 0.08–0.18 W m^{-2} reported above: 0.78 W m^{-2}. Studies of magnetic field indicators suggest that changes over the 19th and 20th centuries were more modest than those assumed in the Shapiro et al.

(2011) reconstruction (Lockwood and Owens, 2011; Svalgaard and Cliver, 2010). Also, analysis by Feulner (2011) indicate that temperature simulations driven by such a large solar forcing are inconsistent with reconstructed and observed historical temperatures, while use of a forcing in line with the range presented here are consistent. Hence we do not include this larger forcing within our assessed range. Schrijver et al. (2011) and Foukal et al. (2011) find a RF which is consistent with the RF range given above (0.08–0.18 W m^{-2}).

8.SM.2.3 Satellite Measurements

Multiple space-based measurements made in the past 30 years (Brueckner et al., 1993; Rottman et al., 1993) show SC variations of ~50% at ~120 nm, ~10% near 200 nm and ~3% near 300 nm. The UV variations account for ~30% of the SC TSI variations, while ~70% are produced by the visible and infrared (Rottman, 2006). AR4, based also on these measurements, reported changes along the SC of ~1.3% at 200 to 300 nm and ~0.2% at 315 to 400 nm. The Spectral Irradiance Monitor (SIM) on board of the Solar Radiation and Climate Experiment (SORCE) measurements (Harder et al., 2009) suggest that over SC 23 declining phase, the 200–400 nm UV flux decreased by ~10 times more than expected from prior observations and model calculations and in phase with the TSI trend, while surprisingly the visible presents an opposite trend. However, SIM's solar spectral irradiance measurements from April 2004 to December 2008 and inferences of their climatic implications are incompatible with the historical solar UV irradiance database, coincident solar proxy data, current understanding of the sources of solar irradiance changes, and empirical climate change attribution results, but are consistent with known effects of instrument sensitivity drifts; thus what seems to be needed is improved characterization of the SIM/SORCE observations and extreme caution in studies of climate and atmospheric change (Haigh et al., 2010) until additional validation and uncertainty estimates are available (DeLand and Cebula, 2012; Lean and DeLand, 2012).

8.SM.3 Synthesis (Global Mean Temporal Evolution)

8.SM.3.1 Summary of Radiative Forcing by Species and Uncertainties

Table 8.SM.2: Radiative forcing (RF) by emitted components as shown in Figure 8.17c. The RF values are made consistent with Table 8.9. For emissions of CO_2, CH_4, CO, NMVOC and NO_X the influence on CO_2, CH_4 and ozone the values are based on Stevenson et al. (2012). The split between NO_X and NH_3 of 40/60 on the RF of nitrate is from Shindell et al. (2009). The BC and OC from biomass burning is set to +0.2 and –0.2, respectively and thus a net RF of biomass burning of 0.0 in line with Table 8.9. BC ari is RF of BC from aerosol-radiation interaction, formerly denoted as direct aerosol effect. Unlike in AR4 (Table 2.13) the N_2O influence on RF of ozone has been set to zero, due to insufficient quantification of this and particularly the vertical profile of the ozone change.

	CO_2	CH_4	N2O	CFCs/HCFCs	HFCs/PFCs/SF_6	BC ari	BC snow	OC	O_3	H_2O(S)	Nitrate	Sulphate	Aerosol-cloud interaction	Total
Components emitted														
CO_2	1.68													1.680
CH_4	0.018	0.651							0.233	0.07				0.972
N_2O			0.17						0					0.170
CFCs/HCFCs/Halons				0.33					-0.20					0.130
HFCs/PFCs/SF_6					0.03									0.030
CO	0.087	0.067							0.075					0.229
NMVOC	0.033	0.026							0.0455					0.105
NO_X		-0.26							0.15		-0.06			-0.170
NH_3											-0.09	0.01		-0.080
BC						0.5	0.04							0.540
OC								-0.24						-0.240
SO_2												-0.41		-0.410
Aerosols													-0.3	-0.300
SUM	1.82	0.48	0.17	0.33	0.03	0.50	0.04	-0.24	0.30	0.07	-0.15	-0.40	-0.30	

8.SM.4 Emission Metrics

8.SM.4.1 Equations for the Global Warming Potential (GWP)

The Absolute Global Warming Potential (AGWP) is the time-integrated radiative forcing due to a 1 kg *pulse* emission of gas *i* (usually in W m^{-2} kg^{-1}year). The Global Warming Potential (GWP) for gas *i* is obtained by dividing the $AGWP_i$ by the AGWP of a reference gas, normally CO_2:

$$GWP_i(H) = \frac{AGWP_i(H)}{AGWP_{CO_2}(H)} = \frac{\int_0^H RF_i(t)dt}{\int_0^H RF_{CO_2}(t)dt}$$

where H is the time horizon, RF_i is the radiative forcing due to a *pulse* emission of a gas *i* given by $RF_i = A_i R_i$ where A_i is the RF_i per unit mass increase in atmospheric abundance of species i (radiative efficiency), and R_i is the fraction of species *i* remaining in the atmosphere after the pulse emissions. For most species, R_i is based on a simple exponential decay,

$$R_i(t) = \exp\left(-\frac{t}{\tau_i}\right)$$

where τ_i is the lifetime and thus, for these species,

$$AGWP_i(H) = \int_0^H RF_i(t)dt = A_i\tau\left(1 - \exp\left(-\frac{H}{\tau}\right)\right)$$

The AGWP for CO_2 is more complicated, because its atmospheric response time (or lifetime of a perturbation) cannot be represented by a simple exponential decay (Joos et al., 2012). The decay of a perturbation of atmospheric CO_2 following a pulse emission at time *t* is usually approximated by a sum of exponentials (Forster et al., 2007; Joos et al., 2012):

$$R_{CO_2}(t) = a_0 + \sum_{i=1}^{N} a_i \exp\left(-\frac{t}{\tau_i}\right)$$

The $AGWP_{CO2}$ is then (Shine et al., 2005):

$$AGWP_{CO_2}(H) = A_{CO_2}\left\{a_0 H + \sum_{i=1}^{\mathrm{I}} a_\mathrm{i}\tau_\mathrm{i}\left(1 - \exp\left(-\frac{H}{\tau_\mathrm{i}}\right)\right)\right\}$$

8.SM.4.2 Equations for the Global Temperature Change Potential (GTP)

The AGTP can be represented as (Boucher and Reddy, 2008; Fuglestvedt et al., 2010):

$$AGTP_i(H) = \int_0^H RF_i(t)R_T(H - t)dt$$

where R_T is the climate response to a unit forcing and can be represented as a sum of exponentials,

$$R_T(t) = \sum_{i=1}^{M} \frac{c_j}{d_j} \exp\left(-\frac{t}{d_j}\right)$$

where the parameters c_i are the components of the climate sensitivity and d_i are response times. The first term in the summation can crudely be associated with the response of the ocean mixed-layer to a forcing and the higher order terms the response of the deep ocean (Li and Jarvis, 2009). The equilibrium climate sensitivity is given by the equilibrium response to a sustained unit forcing, $\lambda = \Sigma\ c_i$.

The simplest form of R_T is a single response term (M=1) (Shine et al. 2005; Olivié et al., 2012). A better representation of the climate response, however, is two or three terms (M=2, 3) (Boucher and Reddy, 2008;

Li and Jarvis, 2009; Olivié et al., 2012). We use R_T from Boucher and Reddy (2008) which assumes two exponential terms and is based on the HadCM3 model (Table 8.SM.1).

Table 8.SM.3: Parameter values for the response to a pulse of radiative forcing used in the AGTP calculations.

	First Term	Second Term
c_i (K(W m^{-2})$^{-1}$)	0.631	0.429
d_j (years)	8.4	409.5

Using the equations above, the AGTP with a time horizon H for the non-CO_2 greenhouse gases:

$$AGTP_i(H) = A_i \sum_{j=1}^{2} \frac{\tau c_j}{\tau - d_j} \left(\exp\left(-\frac{H}{\tau}\right) - \exp\left(-\frac{H}{d_j}\right) \right)$$

and the AGTP for CO_2 is

$$AGTP_{CO_2}(H) = A_{CO_2} \sum_{j=1}^{2} \left\{ a_0 c_j \left(1 - \exp\left(-\frac{H}{d_j}\right)\right) + \sum_{i=1}^{3} \frac{a_i \tau_i c_j}{\tau_i - d_j} \left(\exp\left(-\frac{H}{\tau_i}\right) - \exp\left(-\frac{H}{d_j}\right)\right)\right\}$$

8.SM.4.3 Indirect Effects of Methane

The GWP for CH_4 in AR4 included the OH feedback as well as effects on tropospheric O_3 and stratospheric H_2O. These effects were included by increasing the direct RF from CH_4 by 25% (due to tropospheric O_3) and 15% (due to stratospheric H_2O). New studies provide updated values and include more effects. By accounting for aerosol responses, Shindell et al. (2009) found that the GWP for CH_4 increased by ~40% while Collins et al. (2010) found that the GTP for methane increased by 5–30% when the effect of O_3 on CO_2 was included. Boucher et al. (2009) included the effect of CO_2 from oxidation of methane from fossil sources and calculate a GWP_{100} higher than given in AR4 (27–28 versus 25). They found that CO_2 oxidation had a larger effect on GTP values and this effect was larger than the direct CH_4 effect for time horizons beyond 100 years.

In AR5 we use updated estimates for the indirect effects of CH_4 on tropospheric O_3; 48% (Sections see 8.3.3 and 8.5.1). Thus, we increase the direct RF of CH_4 by 63% to account for RF from both tropospheric O_3 and stratospheric H_2O. We also present metric values for CH_4 of fossil origin (based on Boucher et al., 2009; Table 8.SM.1). If these metric values are used the carbon emitted as CH_4 must not be included in the CO_2 emissions (which are often based on total carbon content).

8.SM.4.4 The Reference Gas CO_2

The metric values need updating due to new scientific knowledge, but also due to changes in lifetimes and radiative efficiencies caused by changing atmospheric background conditions (Peters et al., 2012; Reisinger et al., 2011). For the reference gas CO_2, changes in $AGWP_{CO2}$ and $AGTP_{CO2}$ will affect the GWP and GTP of all other gases. With increasing CO_2 levels in the atmosphere the marginal radiative forcing is reduced, while at the same time the ocean uptake is reduced and airborne fraction increased (Caldeira and Kasting, 1993). These changes are in opposite directions, but do not totally cancel, and hence lead to changes in $AGWP_{CO2}$ and $AGTP_{CO2}$.

The radiative forcing for CO_2 can be approximated using the expression based on radiative transfer models (Myhre et al., 1998):

$$RF = \alpha \log\left(\frac{C_0 + \Delta C}{C_0}\right)$$

where α=5.35, C_0 is the reference concentration and ΔC is the change from the reference. The radiative efficiency is the change in RF for a change in the atmospheric abundance,

$$A = \frac{\Delta RF}{\Delta C} = \alpha \left(\log\left(\frac{C_0+\Delta C}{C_0}\right) \Big/ \Delta C \right)$$

or if $\Delta C \rightarrow 0$ then the derivative can be used

$$A = \frac{dRF}{d\Delta C}\Big|_{\Delta C=0} = \frac{\alpha}{C_0}$$

At current CO_2 levels (390 ppm) and for ΔC=1 ppm, the radiative efficiency (RE) of CO_2 is 1.37×10^{-05} W m^{-2} ppb^{-1}. The difference between using ΔC = 1 ppm and the derivate is 0.13% (Aamaas et al., 2012). To convert the RE values given per ppbv values to per kg, they must be multiplied by $(M_A/M_i)(10^9/T_M)$ where M_A is the mean molecular weight of air (28.97 kg $kmol^{-1}$), M_i is the molecular weight of species *i*, and T_M is the total mass of the atmosphere, 5.14×10^{18} kg (Aamaas et al., 2012; Shine et al., 2005). For CO_2, using a molecular weight of 44.01 kg $kmol^{-1}$, the RE becomes 1.75×10^{-15} W $m^{-2}kg^{-1}$.

The Impulse Response Function has been updated from AR4 (see footnote a) to Table 2.14 in AR4). Figure 8.SM.3 shows the IRFs from the four previous IPCC assessment reports and the new IRF used in AR5 (which is based on Joos et al., 2012).

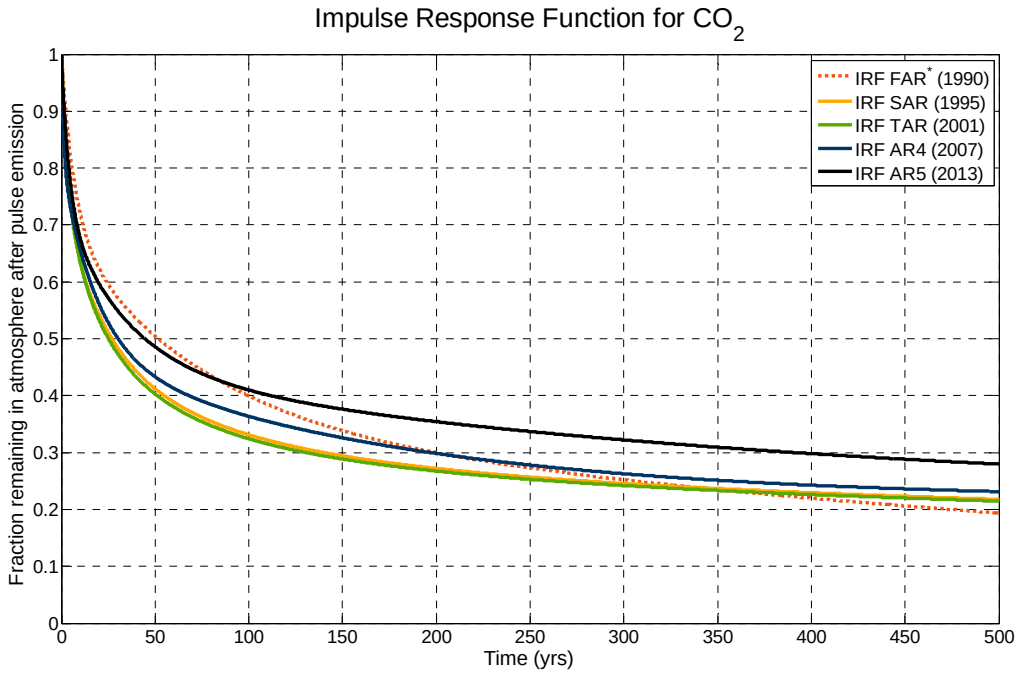

Figure 8.SM.3: The Impulse Response Functions (IRFs) from the five IPCC Assessment Reports. The FAR IRF (dotted) is based on an unbalanced carbon-cycle model (ocean only) and thus is not directly comparable to the others. The SAR IRF is based on the CO_2 response of the Bern model (Bern-SAR), an early generation reduced-form carbon cycle model (Joos et al., 1996), and uses a 10GtC pulse emission into a constant background without temperature feedbacks (Enting et al., 1994). The IRF was not updated for TAR, but a different parameterisation was used in WMO/UNEP Scientific Assessment of Ozone Depletion (1998). The AR4 IRF is based on the Bern2.5CC Earth System Model of Intermediate Complexity (EMIC) (Plattner et al., 2008). A pulse size of 40 GtC is used and includes temperature feedbacks. The AR5 IRF is based on a model intercomparison and uses a pulse size of 100GtC and includes temperature feedbacks (Joos et al., 2012). Apart from FAR, the increasing IRF in each assessment report represents increasing background concentrations and improved models.

In the multi-model exercise by Joos et al. (2012), the multi-model mean R_{CO2} over the first 1000 years is fitted by a sum of exponentials (see equation above) leading to $a_0 = 0.21787$, $a_1 = 0.22896$, $a_2 = 0.28454$, $a_3 = 0.26863$ and the time constants $\tau_1 = 381.33$ yr, $\tau_2 = 34.785$ yr, and $\tau_3 = 4.1237$ yr.
Joos et al. (2012) find the best estimate and uncertainty ranges for the time integrated IRF and AGWP (Table 8.SM.2). The uncertainty range on RE is taken as 10% and a background atmospheric concentration of 389 ppm was used by Joos et al. (2012).

Table 8.SM.4: Mean and uncertainty range for the time-integrated IRF and AGWP (Joos et al, 2012).

	20 Year	100 Year
Time-integrated IRF (yr)		
Mean	14.3	52.4
5–95% Range	12.5–16.0	39.6–65.2
AGWP (10–15 yr W m^{-2} kg^{-1})		
Mean	25.2	92.7
5–95% Range	22.1–28.3	70.1–115

In previous IPCC assessments, GWP values were given for 20, 100 and 500 year time horizons, while here we only use 20 and 100 years. Instead of using GWP values for 500 years we show the response to emissions of some extremely long-lived gases such as PFCs (see Figure 8.SM.4). Once these gases are emitted they stay in the atmosphere and contribute to warming on very long time scales (99% of an emission of PFC-14 is still in the atmosphere after 500 years). For comparison we also include gases with lifetimes of the order of centuries down to a decade. A 1 kg pulse of SF_6 has a temperature effect after 500 years that is almost 40,000 times larger than that of CO_2. The corresponding numbers for CF_4 and C_2F_6 are 14,000 and 23,000, respectively. There are large uncertainties related to temperature responses (as well as the CO_2 response) on time-scales of centuries, but these results nevertheless indicate the persistence and long-lived warming effects of these gases.

One reason for not using a time horizon of 500 years is the increasing uncertainty in radiative efficiency, carbon uptake, and ambiguity in the interpretation of GWP500, especially for gases with short adjustment times relative to the timescale of the CO_2 perturbation. As explained in Section 8.7.1.2, the GWP gives the ratio of two integrals – one of a pulse of a non-CO_2 gas which decays to zero and that of the CO_2 response for which 20–40% of a pulse remains in the atmosphere for centuries. Figure 8.SM.4 also shows that the temperature response to a pulse of the relatively short-lived HFC-134a is close to zero for several centuries before the 500 year time horizon, while the GWP500 is 385. This example highlights how the integrated nature of GWP means that the GWP value at a particular time may give misleading information about the climate impacts at that time as the time scale used in the GWP becomes very different from the residence time of the emitted compound.

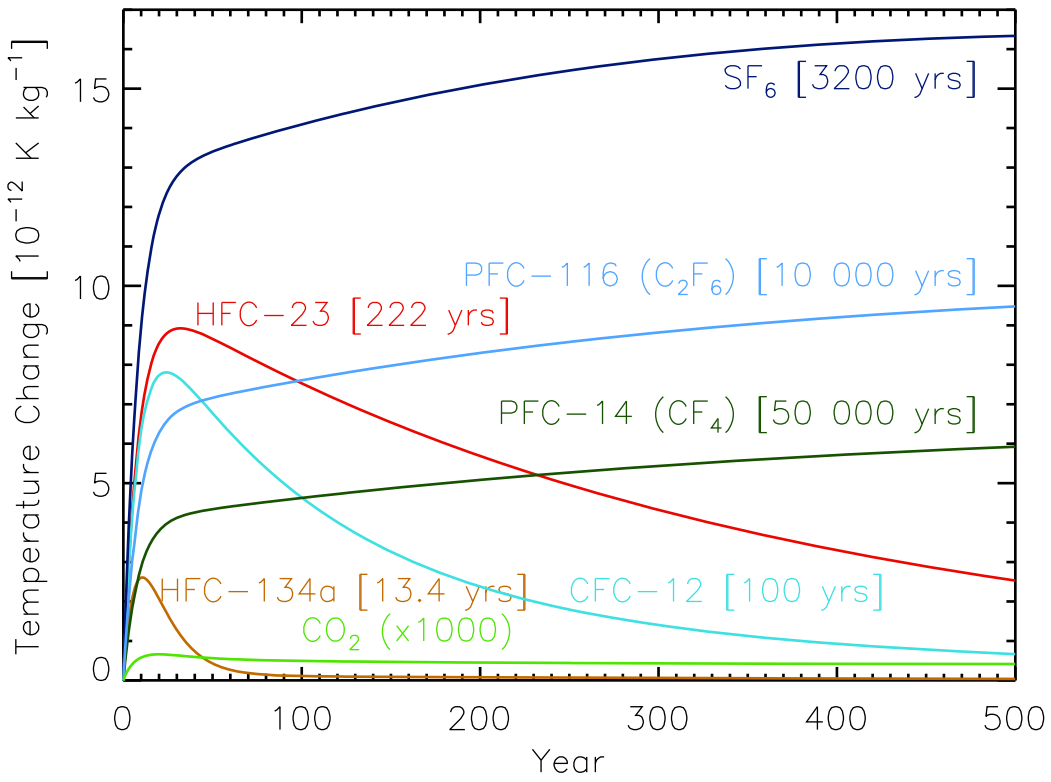

Figure 8.SM.4: Temperature response due to 1-kg pulse emissions of greenhouse gases with a range of lifetimes (given in parentheses). Calculated with a temperature impulse response function taken from Boucher and Reddy (2008) which has a climate sensitivity of 1.06 K (W m^{-2})$^{-1}$, equivalent to a 3.9 K equilibrium response to 2 x CO_2. (Unit for carbon dioxide is kg CO_2).

References

Aamaas, B., Peters, G. and Fuglestvedt, J., 2012. A synthesis of climate-based emission metrics with applications. Earth Syst. Dynam. Discuss. (submitted).

BALIUNAS, S. and JASTROW, R., 1990. EVIDENCE FOR LONG-TERM BRIGHTNESS CHANGES OF SOLAR-TYPE STARS. Nature, 348(6301): 520-523.

Boucher, O., Friedlingstein, P., Collins, B. and Shine, K.P., 2009. The indirect global warming potential and global temperature change potential due to methane oxidation. Environmental Research Letters, 4(4).

Boucher, O. and Reddy, M., 2008. Climate trade-off between black carbon and carbon dioxide emissions. Energy Policy: 193-200.

BRUECKNER, G., EDLOW, K., FLOYD, L., LEAN, J. and VANHOOSIER, M., 1993. THE SOLAR ULTRAVIOLET SPECTRAL IRRADIANCE MONITOR (SUSIM) EXPERIMENT ON BOARD THE UPPER-ATMOSPHERE RESEARCH SATELLITE (UARS). Journal of Geophysical Research-Atmospheres, 98(D6): 10695-10711.

CALDEIRA, K. and KASTING, J., 1993. INSENSITIVITY OF GLOBAL WARMING POTENTIALS TO CARBON-DIOXIDE EMISSION SCENARIOS. Nature, 366(6452): 251-253.

Collins, W.J., Sitch, S. and Boucher, O., 2010. How vegetation impacts affect climate metrics for ozone precursors. Journal of Geophysical Research-Atmospheres, 115.

DeLand, M.T. and Cebula, R.P., 2012. Solar UV variations during the decline of Cycle 23. J. Atm. Solar-Terr. Phys., 77: 225-234.

Enting, I.G., Wigley, T.M.L. and Heimann, M., 1994. Future Emissions and Concentrations of Carbon Dioxide: Key Ocean/Atmosphere/Land Analyses. CSIRO Division of Atmospheric Research Technical Paper no. 31.

Feulner, G., 2011. Are the most recent estimates for Maunder Minimum solar irradiance in agreement with temperature reconstructions? Geophysical Research Letters, 38.

Forster, P., Ramaswamy, V., Artaxo, P., Berntsen, T., Betts, R., Fahey, D.W., Haywood, J., Lean, J., Lowe, D.C., Myhre, G., Nganga, J., Prinn, R., Raga, G., Schulz, M. and Van Dorland, R., 2007. Changes in Atmospheric Constituents and in Radiative Forcing, Climate Change 2007: The Physical Science Basis. Contribution of Working Group I to the Fourth Assessment Report of the Intergovernmental Panel on Climate Change. Cambridge University Press, Cambridge, United Kingdom and New York, NY, USA.

Foukal, P., Ortiz, A. and Schnerr, R., 2011. Dimming of the 17th century Sun. Astrophysical Journal Letters, 733: L38.

Fuglestvedt, J.S., Shine, K.P., Berntsen, T., Cook, J., Lee, D.S., Stenke, A., Skeie, R.B., Velders, G.J.M. and Waitz, I.A., 2010. Transport impacts on atmosphere and climate: Metrics. Atmospheric Environment, 44(37): 4648-4677.

Gray, L., Beer, J., Geller, M., Haigh, J., Lockwood, M., Matthes, K., Cubasch, U., Fleitmann, D., Harrison, G., Hood, L., Luterbacher, J., Meehl, G., Shindell, D., van Geel, B. and White, W., 2010. SOLAR INFLUENCES ON CLIMATE. Reviews of Geophysics, 48: -.

Haigh, J., Winning, A., Toumi, R. and Harder, J., 2010. An influence of solar spectral variations on radiative forcing of climate. Nature, 467(7316): 696-699.

Hall, J. and Lockwood, G., 2004. The chromospheric activity and variability of cycling and flat activity solar-analog stars. Astrophysical Journal, 614(2): 942-946.

Harder, J., Fontenla, J., Pilewskie, P., Richard, E. and Woods, T., 2009. Trends in solar spectral irradiance variability in the visible and infrared. Geophysical Research Letters, 36: -.

Joos, F., Bruno, M., Fink, R., Siegenthaler, U., Stocker, T. and LeQuere, C., 1996. An efficient and accurate representation of complex oceanic and biospheric models of anthropogenic carbon uptake. Tellus Series B-Chemical and Physical Meteorology, 48(3): 397-417.

Joos, F., R. Roth, J. S. Fuglestvedt, G. P. Peters, I. G. Enting, W. von Bloh, V. Brovkin, E. J. Burke, M. Eby, N. R. Edwards, T. Friedrich, T. L. Frö¶licher, P. R. Halloran, P. B. Holden, C. Jones, T. Kleinen, F. Mackenzie, K. Matsumoto, M. Meinshausen, G.-K. Plattner, A. Reisinger, J. Segschneider, G. Shaffer, M. Steinacher, K. Strassmann, K. Tanaka, A. Timmermann and Weaver, A.J., 2012. Carbon dioxide and climate impulse response functions for the computation of greenhouse gas metrics: A multi-model analysis, Atmos. Chem. Phys. Discuss.,.

Lamarque, J., Bond, T., Eyring, V., Granier, C., Heil, A., Klimont, Z., Lee, D., Liousse, C., Mieville, A., Owen, B., Schultz, M., Shindell, D., Smith, S., Stehfest, E., Van Aardenne, J., Cooper, O., Kainuma, M., Mahowald, N., McConnell, J., Naik, V., Riahi, K. and van Vuuren, D., 2010. Historical (1850-2000) gridded anthropogenic and biomass burning emissions of reactive gases and aerosols: methodology and application. Atmospheric Chemistry and Physics: 7017-7039.

Lean, J. and DeLand, M., 2012. How Does the Sun's Spectrum Vary?. J. Climate, 25: 2555-2560.

Li, S. and Jarvis, A., 2009. Long run surface temperature dynamics of an A-OGCM: the HadCM3 4xCO(2) forcing experiment revisited. Climate Dynamics: 817-825.

Lockwood, M. and Owens, M., 2011. Centennial changes in the heliospheric magnetic field and open solar flux: The consensus view from geomagnetic data and cosmogenic isotopes and its implications. Journal of Geophysical Research-Space Physics, 116.

Myhre, G., Highwood, E.J., Shine, K.P. and Stordal, F., 1998. New estimates of radiative forcing due to well mixed greenhouse gases. Geophysical Research Letters, 25(14).

Olivié, D.J.L., Peters, G. and Saint-Martin, D., 2012. Calibration of a linear response Simple Climate Model. J. Climate, doi: http://dx.doi.org/10.1175/JCLI-D-11-00475.1.

Peters, G., Reisinger, A., Fuglestvedt, J. and Meinshausen, M., 2012. Dependence of Global Warming Potentials on constant and variable background concentrations. Environmental Research Letters: (submitted).

Plattner, G.K., Knutti, R., Joos, F., Stocker, T.F., von Bloh, W., Brovkin, V., Cameron, D., Driesschaert, E., Dutkiewicz, S., Eby, M., Edwards, N.R., Fichefet, T., Hargreaves, J.C., Jones, C.D., Loutre, M.F., Matthews, H.D., Mouchet, A., Mueller, S.A., Nawrath, S., Price, A., Sokolov, A., Strassmann, K.M. and Weaver, A.J., 2008. Long-term climate commitments projected with climate-carbon cycle models. Journal of Climate, 21(12): 2721-2751.

Reisinger, A., Meinshausen, M. and Manning, M., 2011. Future changes in global warming potentials under representative concentration pathways. Environmental Research Letters, 6(2): -.

Rottman, G., 2006. Measurement of total and spectral solar irradiance. Space Science Reviews, 125(1-4): 39-51.

ROTTMAN, G., WOODS, T. and SPARN, T., 1993. SOLAR-STELLAR IRRADIANCE COMPARISON EXPERIMENT-1 .1. INSTRUMENT DESIGN AND OPERATION. Journal of Geophysical Research-Atmospheres, 98(D6): 10667-10677.

Schmidt, G., Jungclaus, J., Ammann, C., Bard, E., Braconnot, P., Crowley, T., Delaygue, G., Joos, F., Krivova, N., Muscheler, R., Otto-Bliesner, B., Pongratz, J., Shindell, D., Solanki, S., Steinhilber, F. and Vieira, L., 2011. Climate forcing reconstructions for use in PMIP simulations of the last millennium (v1.0). Geoscientific Model Development, 4(1): 33-45.

Schrijver, C., Livingston, W., Woods, T. and Mewaldt, R., 2011. The minimal solar activity in 2008-2009 and its implications for long-term climate modeling. Geophysical Research Letters, 38.

Shapiro, A., Schmutz, W., Rozanov, E., Schoell, M., Haberreiter, M., Shapiro, A. and Nyeki, S., 2011. A new approach to the long-term reconstruction of the solar irradiance leads to large historical solar forcing. Astronomy & Astrophysics, 529.

Shindell, D.T., Faluvegi, G., Koch, D.M., Schmidt, G.A., Unger, N. and Bauer, S.E., 2009. Improved Attribution of Climate Forcing to Emissions. Science, 326(5953): 716-718.

Shine, K., Fuglestvedt, J., Hailemariam, K. and Stuber, N., 2005. Alternatives to the global warming potential for comparing climate impacts of emissions of greenhouse gases. Climatic Change: 281-302.

Stevenson, D.S., Young, P.J., Naik, V., Lamarque, J.-F., Shindell, D.T., Skeie, R., Dalsoren, S., Myhre, G., Berntsen, T., Folberth, G.A., Rumbold, S.T., Collins, W.J., MacKenzie, I.A., Doherty, R.M., Zeng, G., Noije, T.v., Strunk, A., Bergmann, D., Cameron-Smith, P., Plummer, D., Strode, S.A., Horowitz, L., Lee, Y.H., Szopa, S., Sudo, K., Nagashima, T., Josse, B., Cionni, I., Righi, M., Eyring, V., Bowman, K.W. and Wild, O., 2012. Tropospheric ozone changes, attribution to emissions and radiative forcing in the Atmospheric Chemistry and Climate Model Inter-comparison Project (ACCMIP). ACP/GMD Inter-Journal SI, Submitted.

Svalgaard, L. and Cliver, E., 2010. Heliospheric magnetic field 1835-2009. Journal of Geophysical Research-Space Physics, 115.

van Vuuren, D., Edmonds, J., Kainuma, M., Riahi, K. and Weyant, J., 2011. A special issue on the RCPs. Climatic Change, 109(1-2): 1-4.

Vieira, L., Solanki, S., Krivova, N. and Usoskin, I., 2011. Evolution of the solar irradiance during the Holocene. Astronomy & Astrophysics, 531.

Wright, J.T., 2004. Do we know of any Maunder minimum stars? Astronomical J., 128: 1273-1278.